Journal of Alloys and Compounds 520 (2012) 232–237

Contents lists available at SciVerse ScienceDirect

Journal of Alloys and Compounds

journal homepage: www.elsevier.com/locate/jallcom

Influence of potential, deposition time and annealing temperature on photoelectrochemical properties of electrodeposited iron oxide thin films

Sikandar H. Tamboli [a], Gul Rahman [a,b], Oh-Shim Joo [a,*]

[a] Clean Energy Research Center, Korea Institute of Science and Technology (KIST), Seongbuk-gu, Seoul 130-650, Republic of Korea
[b] School of Science, University of Science and Technology, 52 Eoeun dong, Yuseong-gu, Daejeon 305-333, Republic of Korea

ARTICLE INFO

Article history:
Received 24 October 2011
Received in revised form
27 December 2011
Accepted 4 January 2012
Available online 13 January 2012

Keywords:
Electrodeposition
Hematite
Thin film
Photoelectrochemical cell

ABSTRACT

Nanostructured iron oxide thin films have been prepared by electrodeposition technique and annealed at various temperatures. The effect of deposition potential, deposition time and annealing temperature on photoelectrochemical (PEC) properties of α-Fe_2O_3 thin films was studied. The (1 0 4) and (1 1 0) peak presence in X-ray diffraction patterns confirms α-Fe_2O_3 phase formation. The transition on surface morphology from nanosheets to elongated dumbbell shaped nanoparticles occurred that can be attributed to annealing temperature varied from 400 to 700 °C. Optical band gap variation was observed due to annealing temperature. It was found that increment in film thickness increases the photocurrent from 253 μA/cm^2 to 488 μA/cm^2 at 0.4 V vs Ag/AgCl.

1. Introduction

Hematite (α-Fe_2O_3) is an attractive semiconductor material for photoelectrochemical and photocatalytic purposes due to its stability, benign nature, abundance and environmental compatibility. It is an *n*-type semiconductor which is stable in most electrolytes at pH > 3. It has a band gap 2–2.2 eV which is sufficient to utilize approximately 40% of the incident sunlight for splitting water into oxygen and hydrogen [1,2]. Numerous techniques have been reported for α-Fe_2O_3 thin films deposition such as atmospheric pressure chemical vapor deposition (APCVD) [3], chemical vapor deposition (CVD) [4], low-pressure metallorganic chemical vapor deposition (MOCVD) [5], plasma-enhanced chemical vapor deposition (PECVD) [6], atomic layer deposition [7], spray pyrolysis [8], ultrasonic spray pyrolysis [9], as well as with those prepared by other electrochemical methods [10,11].

Surface morphology of deposited thin film plays important role in PEC property. Kay et al., found dendritic nanostructure with more finely divided branches toward the surface of the film by atmospheric pressure chemical vapor deposition (APCVD) which has given efficient photoelectrode [12]. Effects of deposition angle variation on surface morphology and its PEC performance was studied by Hahn and his co-workers [13]. Beermann et al., has found higher efficiency in hematite electrodes with vertical oriented nanorods than nanostructured spherical morphological electrode [14].

The bottleneck of above mentioned deposition techniques is its high cost. To convert solar energy to chemical energy, the production cost should be less than the other alternatives such as photovoltaic driven electrolyzers or biomass reforming. Electrodeposition is one of the cost effective deposition technique as well as it has capability to deposit thin film at low temperature. Number of researchers has used electrodeposition as deposition technique aiming for various studies [15–17]. There are so many parameters which can affect film properties like reagents, reagent solution concentration, pH of solution, deposition temperature, potential, time, annealing temperature as well as durations. These parameters ultimately reflect variation in film's performance.

In this work, our aim was to study the effects of deposition potential, time (thin film thickness), annealing temperature and durations on the thin film properties and finally on PEC performance.

2. Experimental details

α-Fe_2O_3 thin films were prepared by using 3 M NH_4Cl (Junsei chemical co. Ltd., Japan) and 0.02 M $FeCl_2 \cdot 4H_2O$ (Kanto chemical co. Ltd., Japan) as reagents with 99.5% purity. 1 M NaOH solution was used to adjust the reagent solution pH to 7.52. All solutions were prepared in ultra-pure triply distilled water. Solution was purged with argon during dissolving the reagents, film deposition and photocurrent measurement. The deposition were performed in a conventional three electrode cell using a scanning potentiostat (IviumStat Technologies, Netherlands) with fluorine doped tin oxide (FTO) coated glass plate (1 cm × 1.5 cm) as working electrode, a platinum plate (1.5 cm × 1.5 cm) as counter electrode, Ag/AgCl/NaCl electrode as

* Corresponding author. Tel.: +82 29585215; fax: +82 29585219.
E-mail address: joocat61@gmail.com (O.-S. Joo).

0925-8388/$ – see front matter © 2012 Elsevier B.V. All rights reserved.
doi:10.1016/j.jallcom.2012.01.028

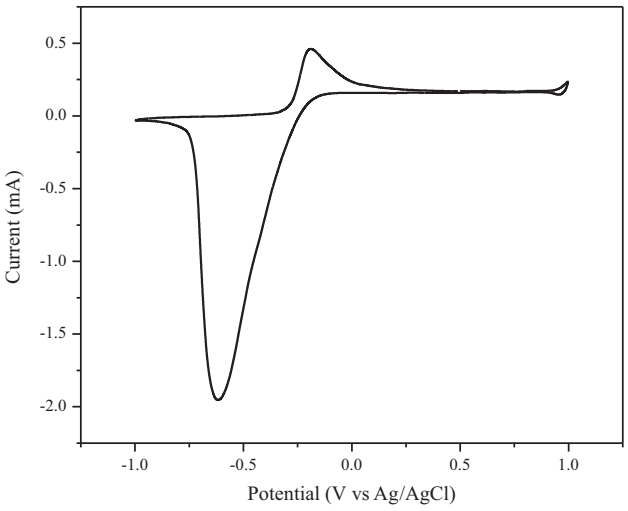

Fig. 1. Cyclic voltammogram of iron precursor solution at 50 mV s^{-1}.

the reference electrode. All electrodeposition potentials were measured with reference to the potential of an Ag/AgCl/NaCl reference electrode. Prior to deposition, the glass substrates were rinsed and sonicated in soap solution, ethanol and triply distilled water for 15 min in each. These cleaned substrates were used for thin film deposition.

Hematite thin film was prepared at different deposition potentials (−0.2, 0.2, 0.4, 0.45 and 0.5 V) and annealed at different temperatures (400, 500, 600 and 700 °C). Film thickness was controlled by changing depositing time for 10, 20, 30 and 40 min. Uniform, smooth Fe_2O_3 films were obtained under optimized conditions which were well adherent to the substrates. To study the annealing duration effect on Fe_2O_3 thin films, thin films were annealed for 10, 30, 60, 120, 240 min.

X-ray diffraction (XRD) data of the electrodeposited α-Fe_2O_3 samples were recorded using X-ray diffractometer (XRD-6000, Shimadzu, Japan) with CuKα radiation (λ = 1.542 Å). Uv-Vis spectrophotometer (Cary-5000, VARIAN) was used for thin film optical absorbance measurements. Field-emission scanning electron microscope (FE-SEM) (HITACHI S-4100 model) was utilized to study thin film surface morphology and thickness.

Photoelectrochemical studies of the α-Fe_2O_3 thin films were carried out in a three-armed cell with a platinum wire as the counter electrode, a Ag/AgCl/NaCl electrode as reference electrode, and the hematite film as the working photoelectrode. These photoelectrochemical studies have been performed in 1 M NaOH solution. The electrolyte solution was purged with argon for 10 min prior to each experimental series and then kept under flowing argon during the experiments. Illumination was provided by a 150 W short-arc Xe lamp solar simulator (PEC-L01, Japan). PEC properties of α-Fe_2O_3 thin films was studied by using back illumination.

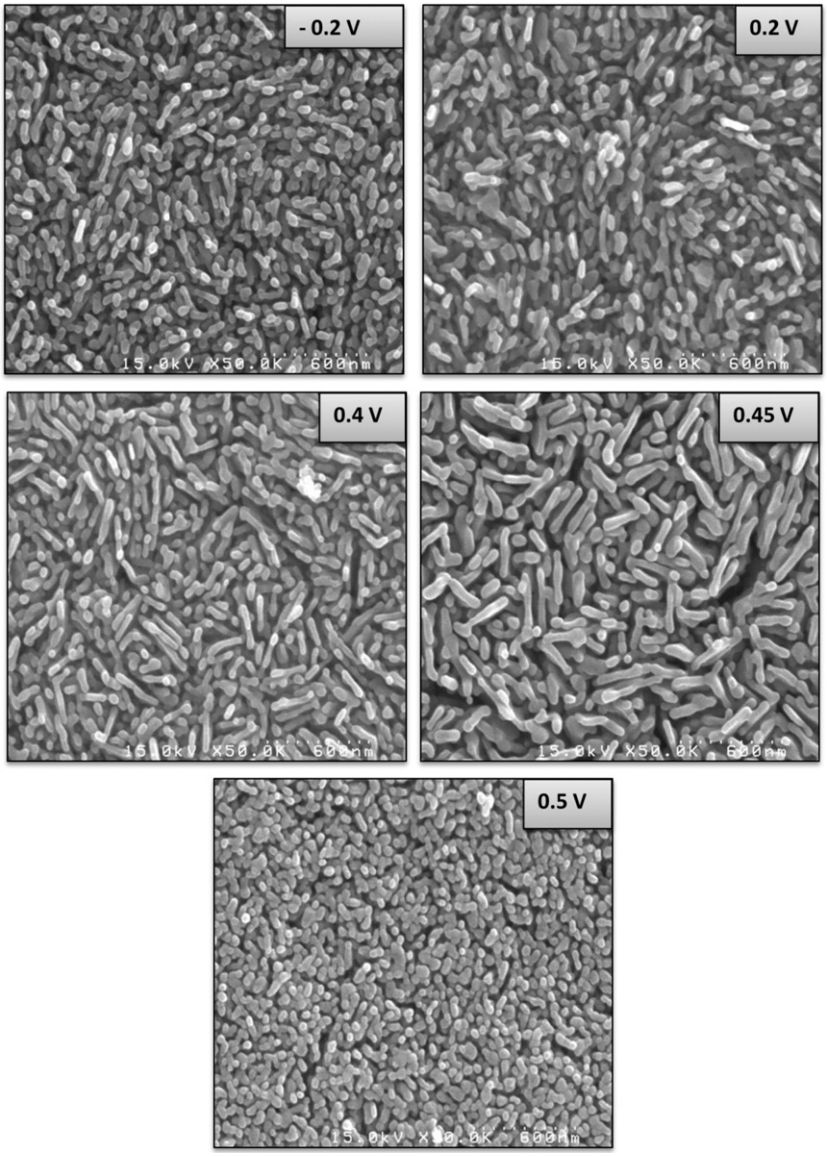

Fig. 2. Surface morphology of α-Fe_2O_3 thin film deposited at various potential.

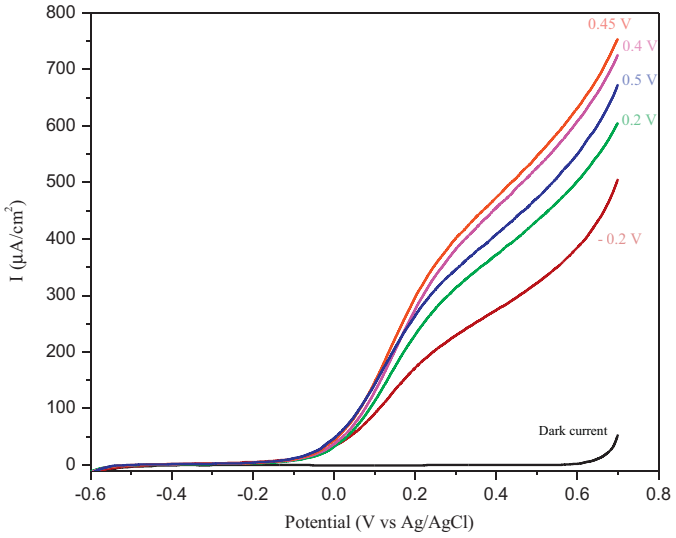

Fig. 3. Current densities of the α-Fe_2O_3 thin films deposited at different potential as a function of the applied potential, V vs Ag/AgCl.

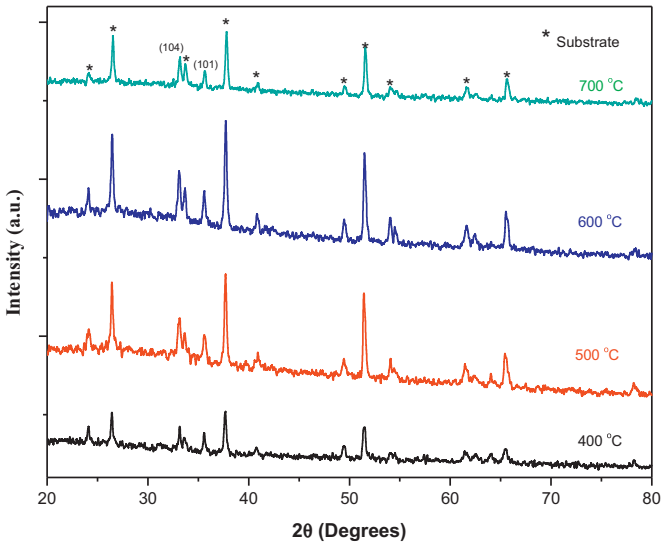

Fig. 4. XRD patterns of α-Fe_2O_3 thin films annealed at various temperatures.

3. Results and discussion

3.1. Potential variation

Fig. 1 shows the cyclic voltammogram in iron precursor solution at 50 mV s^{-1}. During negative sweep Fe^{3+} was reduced to Fe. In reduction region, film deposited at potential −0.58 and −0.7 V. These films showed negligible photo-activity and were not characterized further. Furthermore, in positive sweep films were deposited by electrochemical oxidation of Fe^{2+} ions to Fe^{3+} ions followed by precipitation of Fe^{3+} ions as iron oxide (ferric hydroxide). Iron oxide deposition at the anode are represented by the following equations [18].

$$Fe^{2+} \leftrightarrow Fe^{3+} + e^- \quad (1)$$

$$Fe^{3+} + 3OH^- \rightarrow Fe(OH)_3\downarrow \quad (2)$$

The films deposited at −0.2, 0.2, 0.4, 0.45 and 0.5 V were highly adherent to substrate and showed high photoelectrochemical activity. The effect of deposition potential on grain size as well as on surface morphology of α-Fe_2O_3 thin film was studied by using SEM images, as shown in Fig. 2. It was found that, as potential increases from −0.2 to 0.45 V, the diameter and length of particles were increased and elongated dumbbell shaped nanoparticles were formed. Furthermore, at higher deposition potential than 0.45 V, morphology turns to granular shape from elongated dumbbell shaped.

In electrodeposition process, depositing adatoms continuously progress through the solution and get discharged onto the electrode at applied potential, due to which electrode undergo cluster formation via critical nucleus creation. These critical nuclei act as nucleation centers for further depositing adatoms. The critical nucleus formation and adatoms propagation through solution strongly depends on the applied potential during electrochemical deposition. At low applied potential (as shown in Fig. 2), the rate of nucleation and adatoms propagation remains slower and takes more time for cluster formation, which extends in bigger grain formation (in this case elongated dumbbell shaped). On the other hand, at high applied potential (0.5 V in Fig. 2), nucleation and adatoms propagation rate remains high which increases the number of nuclei, which grow separately and forms smaller grain size (granular shape) [19].

Fig. 3 depicts the photocurrent of the α-Fe_2O_3 thin films deposited at different potential. It was observed that photocurrent increases with increase in deposition potential. α-Fe_2O_3 thin film deposited at −0.2 V and 0.45 V showed 273 μA/cm^2 and 473 μA/cm^2 (at 0.4 V vs Ag/AgCl) respectively. However, film deposited at higher potential than 0.45 V showed reduction in photocurrent. These photocurrent variations are mainly due to the variation in grain size. The large grain size gives high photocurrent due to increase in absorption which would permit holes generation closer to the semiconductor-liquid junction [20].

It is evident that the photocurrent variation correlates with electrode surface morphology via change in deposition potential. It increases with increase in potential up to 0.45 V, the electrodes deposited at these potential shows increase in length and diameter in to dumbbell shaped nanoparticles and results higher photocurrent while turning the surface morphology from elongated dumbbell shape into granular form shrinks the photocurrent. An electrode having larger grain size reduces the grain boundaries, which provides low electron–hole recombination, reflects high photocurrent, whereas smaller grain size increases the grain

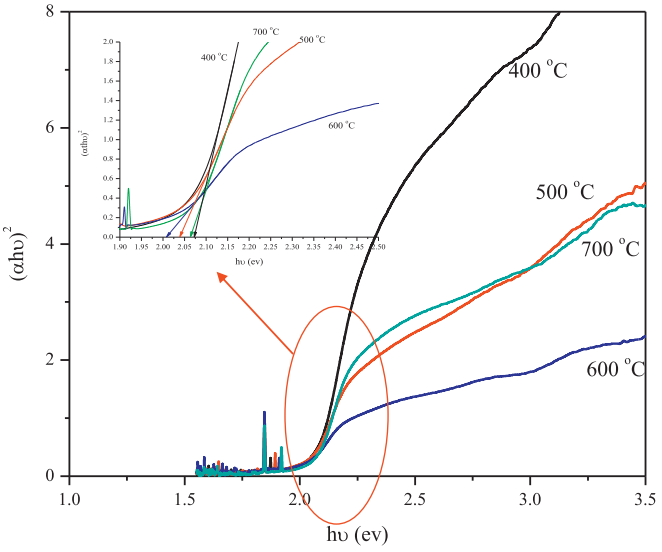

Fig. 5. Graph of $(\alpha th\upsilon)^2$ as a function of $h\upsilon$ for optical band gap.

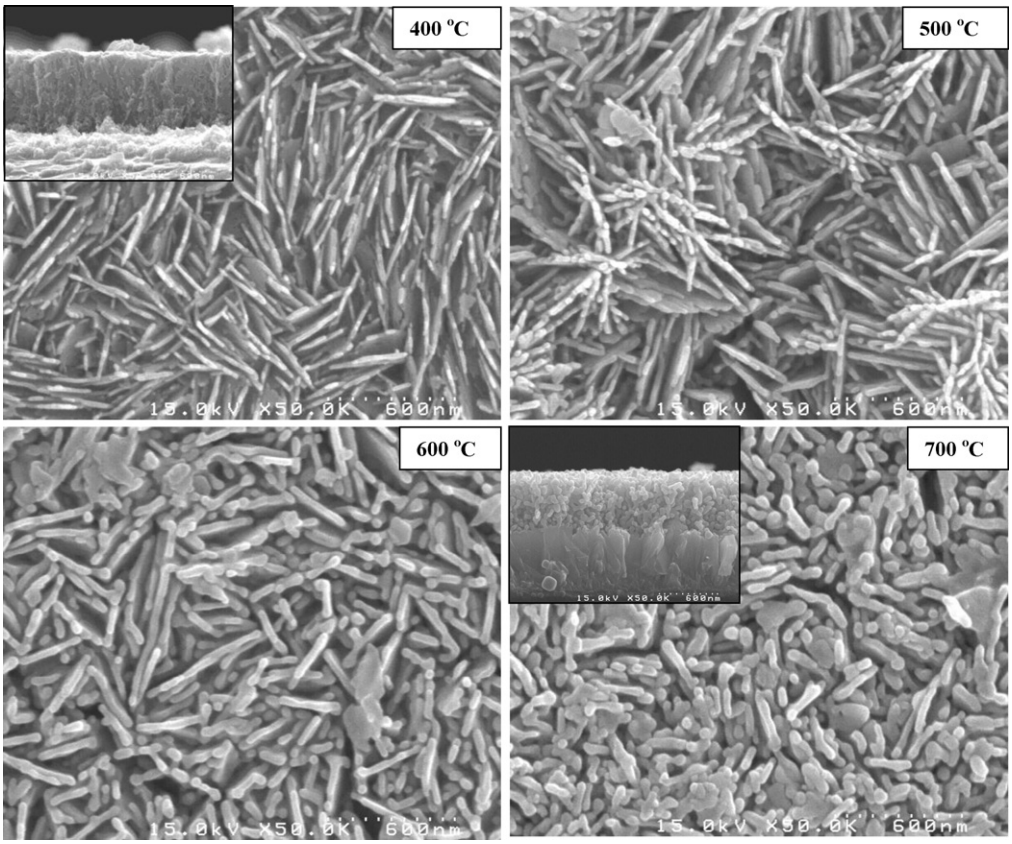

Fig. 6. Surface morphology of α-Fe_2O_3 thin film annealed at various temperatures. Vertical cross-section image in inset.

boundaries as well as electron–hole recombination. Due to high electron–hole recombination photocurrent becomes low [21].

3.2. Temperature effect

As deposited iron oxide films were converted into α-Fe_2O_3 thin films by annealing for 4 h. The effect of annealing temperature on crystal structure was analyzed by XRD patterns. Fig. 4 shows the XRD patterns of α-Fe_2O_3 thin films annealed at various temperatures (400–700 °C) for 4 h. The (1 0 4) and (1 1 0) peaks were observed which confirms the α-phase formation (JCPDS data no. 89-0599). It is seen that, annealing temperature increases the peak intensity of α-Fe_2O_3, which indicate that the crystallinity of film increases with annealing temperature [22].

Fig. 5 gives the plot of $(\alpha th\upsilon)^2$ as a function of $h\upsilon$. From the absorption data, the band gap energy was calculated using the formula:

$$\alpha = \frac{[\alpha_0(h\upsilon - E_g)^n]}{h\upsilon} \quad (3)$$

where, 'E_g' is the separation between bottom of the conduction band and top of the valence band, α is the absorption of thin film and α_0 is the absorption Coefficient, '$h\upsilon$' is the photon energy and 'n' is a constant. The value of n depends on the probability of transition; it takes values as 1/2, 3/2, 2 and 3 for direct allowed, direct forbidden, indirect allowed and indirect forbidden transition, respectively. Small reduction in optical band gap was observed due to increase in annealing temperature such as 2.07, 2.06, 2.01 and 2.04 eV for 400, 500, 600 and 700 °C respectively. All the optical band gap values were in reported range [21,22].

The effect of annealing temperature enhancement on surface morphology is shown in Fig. 6. Nanosheets like morphology was observed at low annealing temperature (400 °C), whereas this morphology turns into elongated dumbbell shaped nanoparticles due to increase in annealing temperature from 400 to 700 °C. The formation of nanosheets and nanoparticles were confirmed by taking vertical cross section SEM image, as shown in inset in Fig. 6. The increase in diameter of nanoparticles (width of nanosheets) found to increase with increase in annealing temperature from 20 to 38 nm for 400–700 °C.

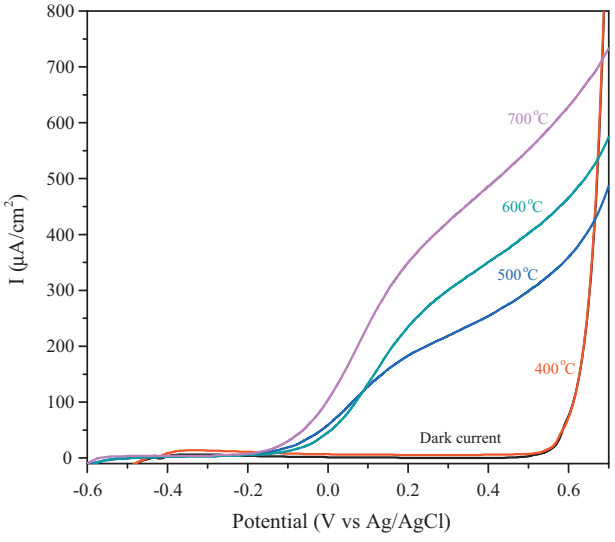

Fig. 7. Current densities of the α-Fe_2O_3 thin films annealed at various temperatures as a function of the applied potential, V vs Ag/AgCl.

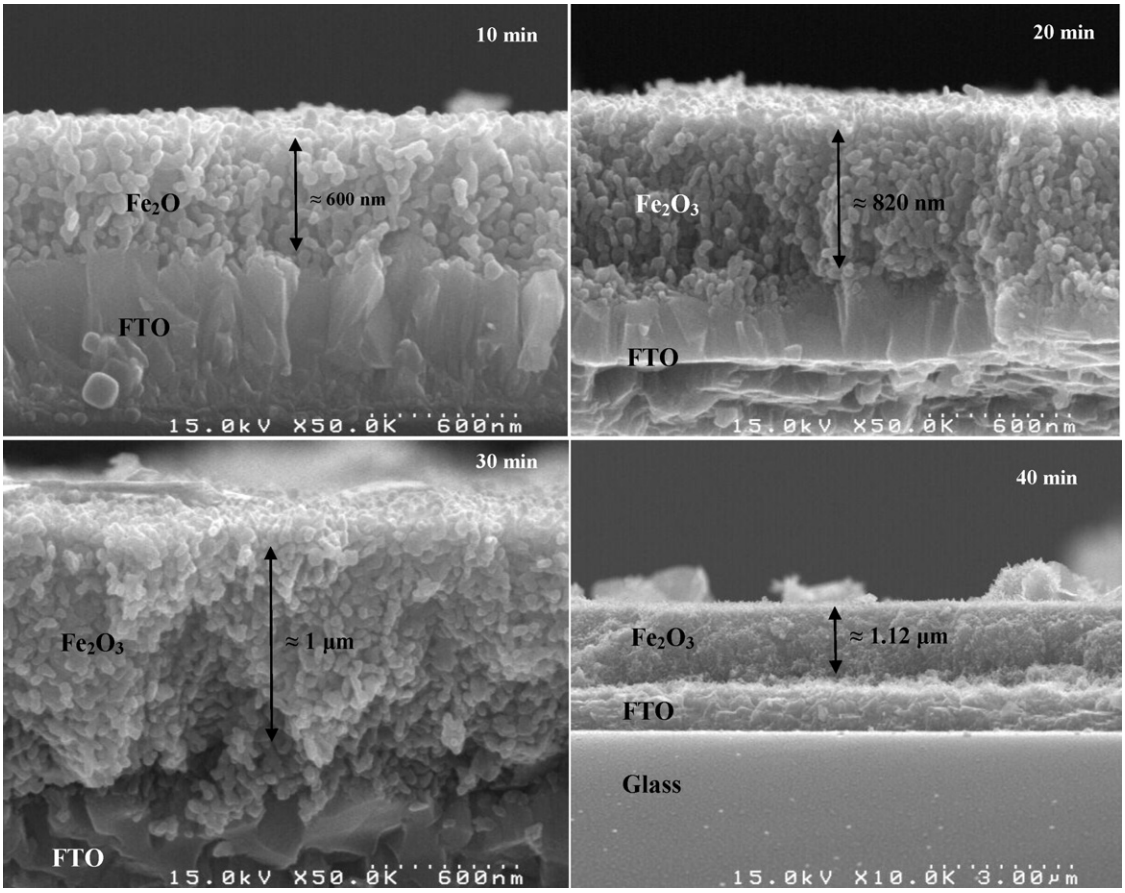

Fig. 8. Vertical cross section of α-Fe_2O_3 thin films deposited at different time.

The effect of annealing temperature on photochemical properties of α-Fe_2O_3 thin film is shown in Fig. 7. It was oberved that α-Fe_2O_3 thin film annealed at 400 °C showed low photocurrent, while it increases with annealing temperature. Increase in photocurrent with annealing temperature is due to the crystallinity improvement as well as elimination of trapped excess vacancies i.e., voids within the film [13,23]. These voids reduction is interrelated with photocurrent enhancement. This reduction in void formation at high temperature can be observed in FE-SEM image of α-Fe_2O_3 thin films in Fig. 6. It shows that, at high annealing temperature grain size increases and voids decreases. This grain size increment caused to reduce the grain boundaries as well as electron–hole recombination [21]. This reduction in electron–hole recombination reflects photocurrent improvement with annealing temperature.

The effect of annealing duration on photoelectrochemical properties of α-Fe_2O_3 thin films was studied. The photocurrent values of α-Fe_2O_3 thin film annealed at 700 °C for different durations are tabulated in Table 1. Photocurrent of α-Fe_2O_3 thin film was found to increase with increase in annealing duration. The photocurrent density achieved 461 μA/cm^2 at 0.4 V vs Ag/AgCl after 240 min of annealing. The resistance of the substrate was slightly increased.

Table 1
The values of photocurrent variation with α-Fe_2O_3 thin film annealing duration.

Annealing duration (min)	Photocurrent (μA/cm^2) at 0.4 V vs Ag/AgCl
10	156
30	271
60	335
120	404
240	461

3.3. Deposition time

Time of film deposition mainly affects on its thickness. As deposition time increases, an increase in thickness of α-Fe_2O_3 thin films was observed. The thickness of film was measured by taking vertical cross section SEM. Fig. 8 shows the vertical cross section of Fe_2O_3 thin films deposited at different time intervals. It was observed that, the deposition time effect on film thickness as well as photocurrent. The photocurrent increases with film thickness from 600 nm to 1120 nm (253 μA/cm^2–488 μA/cm^2 at 0.4 V vs Ag/AgCl).

In this study, photocurrent was measured by illuminating the back side of the film. During illumination, light absorption takes place including blue and red region of the visible spectrum. The longer wavelength (red) have similar effect in thin as well as relatively thicker film, whereas short wavelength (blue), which produces most of the charge carriers and get absorbed comparatively more in the thicker films as compared to the thinner films. As a result thicker electrodes absorb more photons and hence, produce high photocurrent for water oxidation [24–26].

4. Conclusion

α-Fe_2O_3 thin films were successfully prepared using electrodeposition technique and were studied for photoelectrochemical cell application. The variations in thin film deposition potential, annealing temperature and film thickness played a crucial role in photocurrent variation via thin film modifications. Surface morphology modification is more dominant factor in photoelectrochemical properties of α-Fe_2O_3 thin films, which is interrelated with electron–hole recombination phenomenon. The elongated dumbbell shaped surface morphology of α-Fe_2O_3 thin films is the

optimum morphology for photoelectrochemical cell application than nanosheets or granular morphology. The surface morphological variation and its effect on device performance is mainly concerned with surface engineering.

Acknowledgement

This work was funded by the "Hydrogen Energy R & D Center" one of the 21st Century frontier R & D Programs, funded by Ministry of Science and Technology of Korea.

References

[1] K. Sivula, F.L. Formal, M. Gratzel, ChemSusChem 4 (2011) 432.
[2] Y.S. Hu, A.K. Shwarsctein, A.J. Forman, D. Hazen, J.N. Park, E.W. McFarland, Chem. Mater. 20 (2008) 3803.
[3] I. Cesar, A. Kay, J.A.G. Martinez, M. Gratzel, J. Am. Chem. Soc. 128 (2006) 4582.
[4] T. Maruyama, T. Kanagawa, J. Electrochem. Soc. 143 (1996) 1675.
[5] K. Shalini, G.N. Subbanna, S. Chandrasekaran, S.A. Shivashankar, Thin Solid Films 424 (2003) 568.
[6] E.T. Lee, B.J. Kim, G.E. Jang, Thin Solid Films 341 (1999) 73.
[7] M. Lie, H. Fjellvag, A. Kjekshus, Thin Solid Films 488 (2005) 74.
[8] A.A. Akl, Appl. Surf. Sci. 233 (2004) 307.
[9] A. Duret, M. Grätzel, J. Phys. Chem. B 109 (2005) 17184.
[10] D. Lincot, Thin Solid Films 487 (2005) 40.
[11] G. Zotti, G. Schiavon, S. Zecchin, U. Casellato, J. Electrochem. Soc. 145 (1998) 385.
[12] A. Kay, I. Cesar, M. Gratzel, J. Am. Chem. Soc. 128 (2006) 15714.
[13] N.T. Hahn, H. Ye, D.W. Flaherty, A.J. Bard, C.B. Mullins, ACS Nano 4 (2010) 1977.
[14] N. Beermann, L. Vayssieres, S.E. Lindquist, A. Hagfeldt, J. Electrochem. Soc. 147 (2000) 2456.
[15] R.L. Spray, K.S. Choi, Chem. Mater. 21 (2009) 3701.
[16] A.K. Shwarsctein, Y.S. Hu, A.J. Forman, G.D. Stucky, E.W. McFarland, J. Phys. Chem. C 112 (2008) 15900.
[17] R. Schrebler, C. Llewelyn, F. Vera, P. Cury, E. Munoz, R. Rio, H.G. Meier, R. Cordova, E.A. Dalchiele, Electrochem. Solid-State Lett. 10 (2007) D95–D99.
[18] M.S. Wu, R.H. Lee, J. Electrochem. Soc. 156 (2009) A737.
[19] R.K. Pandey, S.N. Sahu, S. Chandra, Handbook of Semiconductor Electrodeposition, Marcel Dekker, Inc, New York, 1996.
[20] K. Sivula, R. Zboril, F.L. Formal, R. Robert, A. Weidenkaff, J. Tucek, J. Frydrych, M. Gratzel, J. Am. Chem. Soc. 132 (2010) 7436.
[21] J.A. Glasscock, P.R.F. Barnes, I.C. Plumb, A. Bendavid, P.J. Martin, Thin Solid Films 516 (2008) 1716.
[22] A. Boudjemaa, S. Boumaza, M. Trari, R. Bouarab, A. Bouguelia, Int. J. Hydrogen Energy 34 (2009) 4268.
[23] G. Wang, Y. Ling, D.A. Wheeler, K.E.N. George, K. Horsley, C. Heske, J.Z. Zhang, Y. Li, Nano Lett. 11 (2011) 3503–3509.
[24] X. Qian, X. Zhang, Y. Bai, T. Li, X. Tang, E. Wang, S. Dong, J. Nanoparticle Res. 2 (2000) 191.
[25] B.M. Klahr, A.B.F. Martinson, T.W. Hamann, Langmuir 27 (2011) 461.
[26] R.H. Gonc-alves, B.H.R. Lima, E.R. Leite, J. Am. Chem. Soc. 133 (2011) 6012.